Bull. Mater. Sci., Vol. 38, No. 3, June 2015, pp. 761–768. © Indian Academy of Sciences.

Preparation and characterization of electroless Ni–B/nano-SiO_2, Al_2O_3, TiO_2 and CuO composite coatings

DURSUN EKMEKCİ[1,*] and FERHAT BÜLBÜL[2]

[1]Department of Mechanical Engineering, Engineering and Nature Faculty, Gumushane University, 29100 Gümüşhane, Turkey

[2]Department of Mechanical Engineering, Engineering Faculty, Ataturk University, 25240 Erzurum, Turkey

MS received 5 September 2014; revised 19 December 2014

Abstract. **Ni–B/SiO_2, Al_2O_3, TiO_2 and CuO composite coatings were successfully obtained by the electroless plating technique. Dispersible SiO_2, Al_2O_3, TiO_2 and CuO nanoparticles were co-deposited with electroless Ni–B coating onto AISI-304 steel substrates. Deposits were characterized for its structural properties by X-ray diffraction (XRD). XRD results showed a broad peak of Ni–B and low intensity composite nanoparticle peaks. The surface and cross-section morphology of samples were analysed using a scanning electron microscope (SEM). Surface analysis showed that the incorporation in Ni–B matrix of nano-SiO_2, Al_2O_3, TiO_2 and CuO particles increases the nodularity of composite coatings. The deposits are composed of a columnar structure grown along the vertical direction of the substrate surface. The results also show that electroless nanocomposite coatings tend to have greater microhardness compared with the coating without nanoparticles. The increase in the microhardness of the nanocomposite coatings reported in this study is attributed to an effect of dispersion strengthening of ceramic particles in the Ni–B matrix.**

Keywords. **Electroless Ni–B; nanoparticle; coating; microhardness; SEM; XRD.**

1. Introduction

Electroless Ni–B coating is a new candidate technology for use in a wide range of engineering industries due to its many advantages, such as thickness uniformity, good wear resistance, lubricity, good ductility and corrosion resistance and excellent solderability and electrical properties.[1] To enhance the properties of electroless nickel–boron coating, reinforcement may be added to the solution to produce composite coating. Deposition of the particles depends on the size, shape, density, concentration and technique of suspension in the bath. The type of composite components and the particle size dispersed into the composite matrix determine utilizable properties of nickel–boron composite layers. It can be reinforced with various types of particulates to produce recent multifunctional composite materials. For instance, it has been found that the presentation of hard particles leads to increase in the mechanical and physical properties of electroless Ni–P alloy coating.[2] Many composite coatings are characterized by an amorphous or crystalline Ni–P matrix into which oxides such as SiO_2,[2,3] TiO_2[4–6] and Al_2O_3[7–10] were incorporated. Namely, deposited SiO_2, TiO_2 and Al_2O_3 particles contributed to the increase in the hardness and wear resistance of electroless Ni–P coating.

There is no report on SiO_2, TiO_2, Al_2O_3 and CuO-reinforced electroless Ni–B composite coatings. In the present work, using SiO_2, Al_2O_3, TiO_2 and CuO powders, Ni–B composites were prepared on AISI 304 stainless-steel substrates by the electroless deposition method. Deposits were structurally and morphologically characterized by scanning electron microscopy (SEM) and X-ray diffraction (XRD), because microstructural characterization of the coatings is important as it helps to better understand its macroscopic behaviour by observing the changes occurring at the microscopic level of the coating.

2. Experimental

Table 1 summarily presents the information on the used material and experimental methods. As guided by preliminary studies and a literature survey, controllable parameters and their levels were selected as described in table 1. Electroless Ni–B/SiO_2, Al_2O_3, TiO_2 and CuO composite coatings produced under these experimental conditions were investigated in terms of their morphological and crystallographic properties. Nanoparticle powders used were of the sizes 20 nm–SiO_2, 40 nm–CuO, 30 nm–Al_2O_3 and 30 nm–TiO_2. About 250 ml of electroless Ni–B/SiO_2, Al_2O_3, TiO_2 and CuO solution containing 2.5 g l^{-1} of nanoparticle powder was thoroughly mixed using a mortar. Magnetic stirrer was used to obtain uniform suspension of particles in the solution.

3. Results and discussion

3.1 *Structural analysis of coatings*

XRD result and SEM micrograph for the AISI 304 steel substrate used show the crystal phases of γ-Fe (111) at

*Author for correspondence (dursunekmekci@gumushane.edu.tr)

Table 1. Used material and expeimental methods.

Substrate	AISI 304 austenitic stainless steel (15 × 15 × 5 mm)						
% Chemical composition	C ≤ 0.07; Cr: 18–20; Mn ≤ 2; P: 0.045; Si ≤ 1; Ni: 9; S ≤ 0.03; diğer % Fe						
Surface roughness of substrate, R_a	0.1 μm (at mechanically polishing using SiC emery paper with 1200 mesh grit and then with α-alumina having 0.05 μm grain size)						
Treatment before deposition	Degreasing with acetone, and rinsing with distilled water, and pickling in 15% HCl for 15 s and then washing thoroughly with distilled water and drying in air with a fan						
	The type of coating	Deposition time (min)	Concentration of $NaBH_4$ (g l^{-1})	Concentration of $NiCl_2$ (g l^{-1})	Concentration of $PbNO_3$ (g l^{-1})	Concentration of NaOH (g l^{-1})	Concentration of $NH_2–CH_2–CH_2–NH_2$ (g l^{-1})
Deposition parameters	Ni–B	30	0.6	5	0.00725	45	0.5
	*Ni–B/SiO_2	60	0.3	2.5	0.003625	22.5	0.25
	*Ni–B/TiO_2	60	0.3	2.5	0.003625	22.5	0.25
	*Ni–B/Al_2O_3	60	0.3	2.5	0.003625	22.5	0.25
	*Ni–B/CuO	60	0.3	2.5	0.003625	22.5	0.25
Constant parameters	Bath temperature 95°C, pH 13.5						
Characterization equipment	Jeol 6400 SEM (for morphological analysis), Rigaku D/Max 2000 XRD (for phase structure analysis) Struers Duramin Vickers diamond indenter (for hardness measurement)						

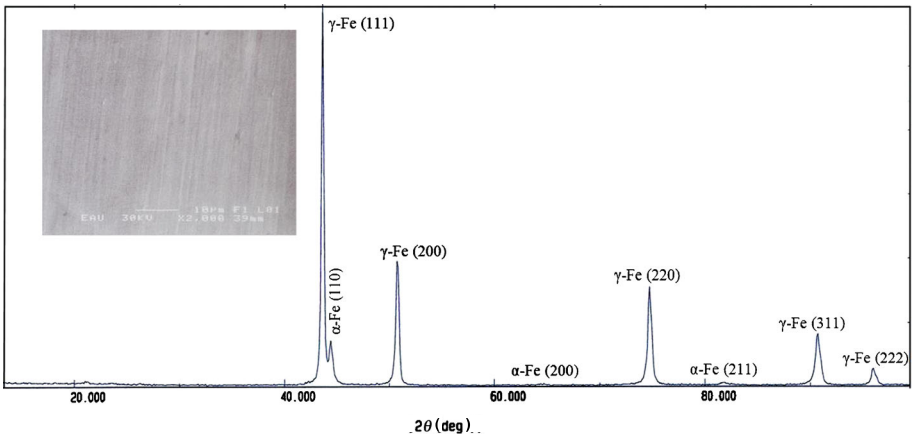

Figure 1. XRD spectrum of AISI 304 stainless-steel substrate.

$2\theta \approx 43.7°$, α–Fe (110) at $2\theta \approx 44.6°$, γ-Fe (200) at $2\theta \approx 50.8°$, α–Fe (200) at $2\theta \approx 64.7°$, γ-Fe (220) at $2\theta \approx 74.7°$, α–Fe (211) at $2\theta \approx 82.1°$, γ-Fe (311) at $2\theta \approx 90.7°$ and γ–Fe (222) at $2\theta \approx 96.1°$ (figure 1). The morphological and the crystallographic variations of electroless Ni–B coatings based onthe employed deposition conditions are discussed below.

The cross-sectional SEM view of the electroless nickel–boron coating is given in figure 2. The electroless nickel–boron coating grows uniformly and regulating columnar in general. The electroless nickel–boron plating thickness was found to be about 5.50 μm. The produced Ni–B coatings were nodular; however, the size of the nodules varied for the non-reinforced and reinforced coatings. These nodules occur in combination of small spherical particles in blackberry-like and cauliflower-like structures. Once nucleation events take place, the Ni–B alloy grains grow into spherical nodules. It may be explained that the spherical nodules are the product of the autocatalytic reaction with sodium borohydride participating in it. This is because the substrates like steel

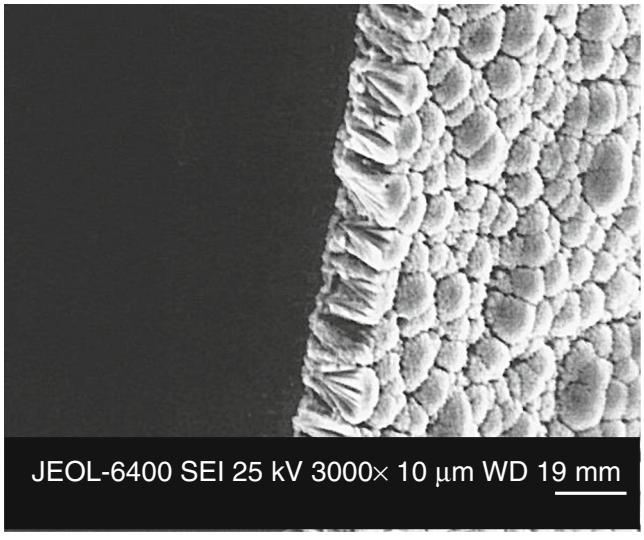

Figure 2. SEM image of electroless Ni–B film cross-section on AISI 304 stainless-steel substrate.

and aluminium become catalytic when a thin nickel deposit is formed over the substrate on immersion in an electroless plating bath. The catalytic sites on the initial deposits act as nucleating sites for additional nodules.

Figure 3 shows the 8000×-SEM images of electroless Ni–B and Ni–B/nanocomposite coatings. SEM investigation indicates that the morphology of the growth surface of the Ni–B coating with columnar structure is blackberry-like. The same morphology has also been observed in the study of Bülbül *et al.*[11] The size of nodule is 0.6 μm for each blackberry of electroless Ni–B coating.

In figure 4, it is seen the SEM images of the surface morphologies of electroless Ni–B and Ni–B/nano-SiO_2 coatings. It is seen that SiO_2 nanoparticles are embedded in the Ni–B matrix via codeposition, and some of the SiO_2 nanoparticles are agglomerated to a certain degree even in the presence of magnetic agitation. The SiO_2 nanoparticles are successfully co-deposited with Ni–B matrix to generate Ni–B/nano-SiO_2 composite coatings in the absence of any surfactants in the plating bath. Figure 4 shows the nodules at a large number on the surfaces. It also has been reported by Rabizadeh and Allahkaram[12] that these spherical nodules are incorporated of SiO_2 nanoparticles with the separation of nickel and boron from electroless Ni–B matrix phase.

In figure 4b, the XRD patterns of as-deposited Ni–B/nano-SiO_2 composite coatings are shown. It is seen that the as-deposited composite coating has amorphous structure. No significant effect compared to Ni–B plating Ni–B/SiO_2 (figure 4b) is observed. The Ni–B/SiO_2 coating partially transforms into a crystalline structure. The grain structure is seen in the form of nodular cauliflower. These grain structures are smaller than blackberry grains compared with the Ni–B

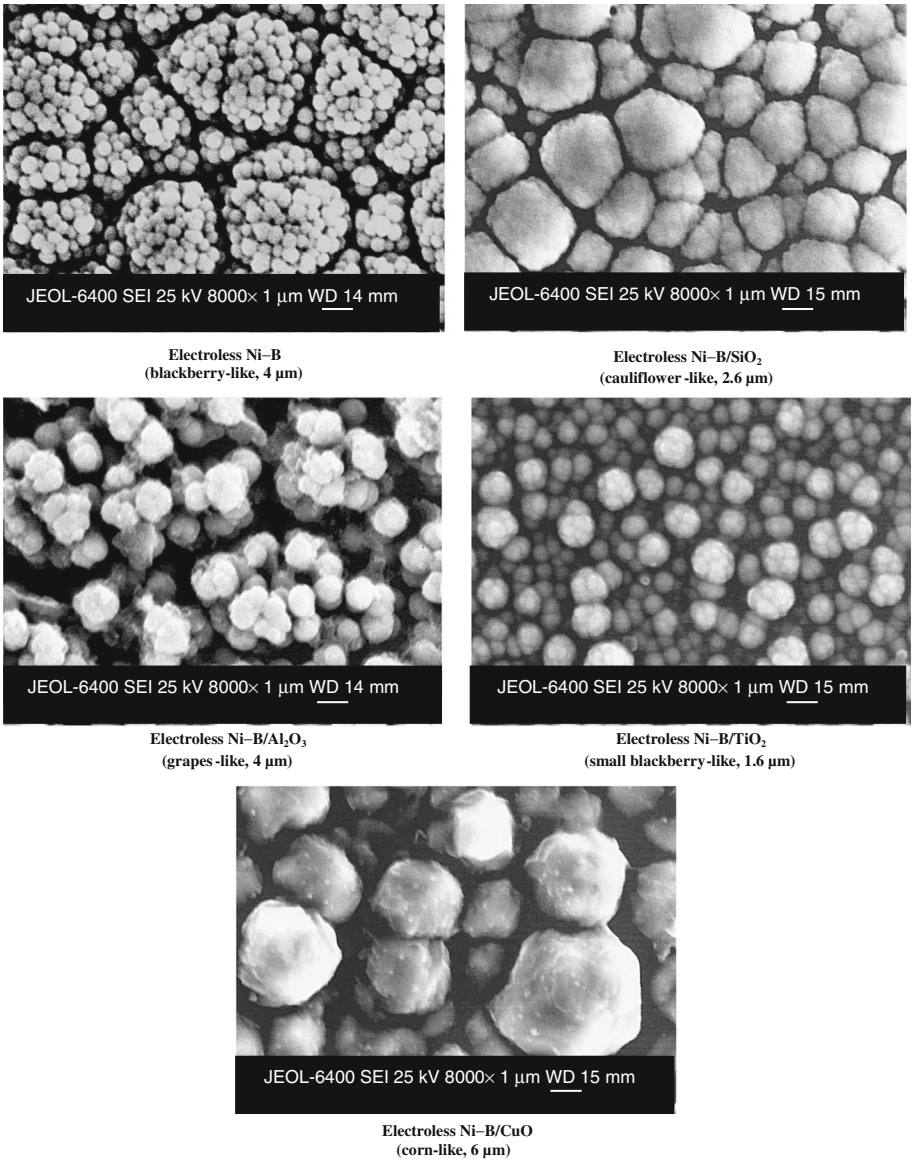

Figure 3. SEM images of electroless Ni–B and Ni–B/nanocomposite coatings.

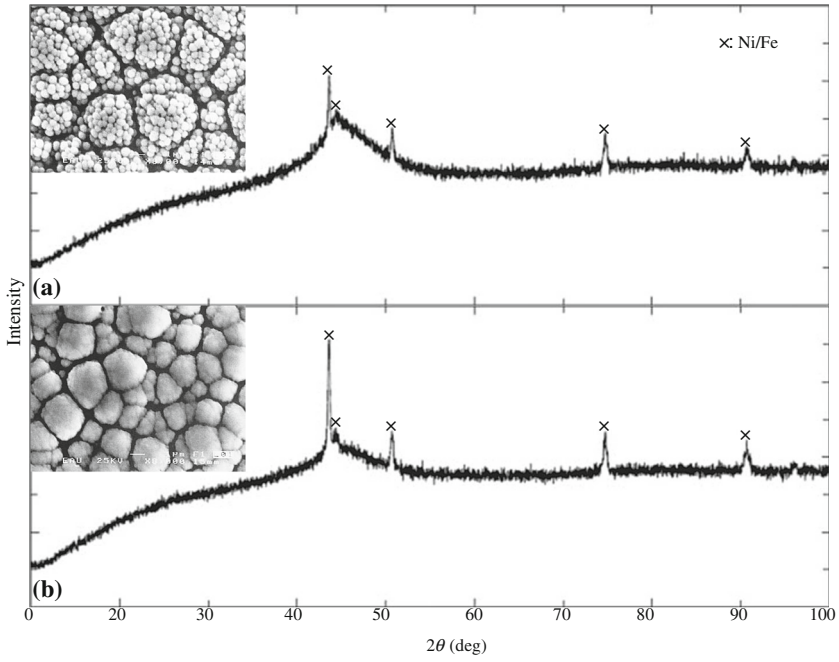

Figure 4. SEM images and XRD spectra of electroless (**a**) Ni–B and (**b**) Ni–B/SiO_2 composite coatings.

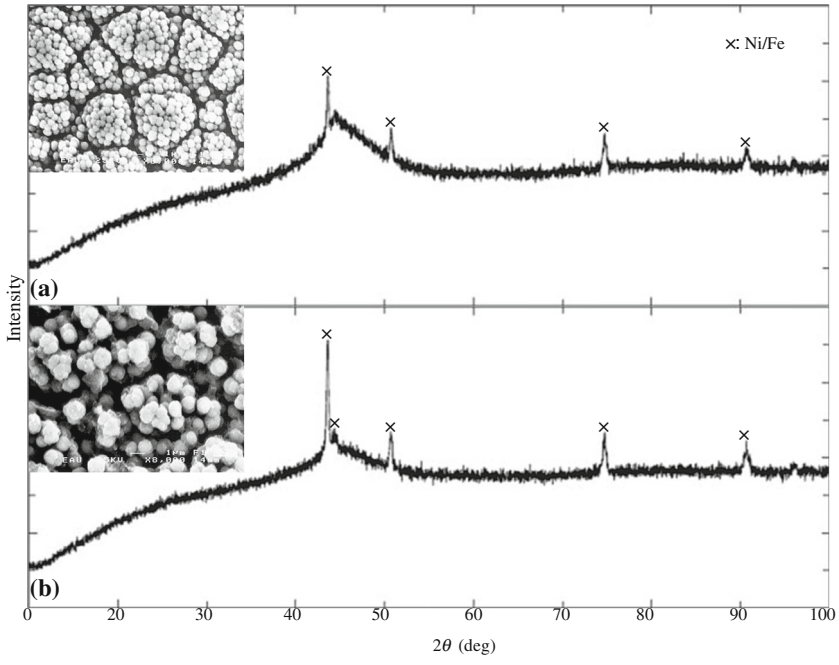

Figure 5. SEM images and XRD spectra of electroless (**a**) Ni–B and (**b**) Ni–B/Al_2O_3 composite coatings.

plating. However, the grain boundaries with reinforcement-nano-SiO_2 particles are filled and the density of the coating increases. XRD result for the Ni–B/SiO_2 coatings signs the phase points Ni/Fe (111) at $2\theta \approx 43.58°$, Ni/Fe (110) at $2\theta \approx 44.36°$, Ni/Fe (200) at $2\theta \approx 50.7°$, Ni/Fe (220) at $2\theta \approx 74.7°$ and Ni/Fe (311) at $2\theta \approx 90.64°$ (figure 5b).

Al_2O_3[7–10] studies show that the addition of alumina particles influences the morphology and properties of the composite coatings (figure 5). It can be seen that while the surface of Ni–B coating is very smooth, the surface of Ni–B/Al_2O_3 composite coating is coarser and there are many nodular protrusions over the surfaces. These nodules

are spherical in shape. The microstructure of Ni–B/Al_2O_3 coating is observed in the form of grapes like. Also it is evident from the micrographs that the alumina particles are distributed throughout the surface although agglomeration is observed in some places. More amount of particle incorporation is seen in the case of electroless Ni–B/Al_2O_3 composite coating. It can be seen that nickel and boron are uniformly distributed in the deposit. More agglomeration of 30-nm particles can be understood from the SEM image of Ni–B/Al_2O_3 composite coating (figure 5b). Nodularity is reduced by higher level of the particle incorporation. Electroless Ni–B/Al_2O_3 deposit exhibits smooth fine nodular morphology with scattered wide nodules which is shown in figure 5b. Incorporation of alumina particles in Ni–B/Al_2O_3 matrix has increased the nodule size. It is evident that the presence of alumina particles is uniformly codeposited in the Ni–B matrix on the surface. All of these reflections correspond to the codeposited aluminium oxide particles present in the composite coating.

In figure 5, the X-ray mapping of as-deposited electroless Ni–B and Ni–B/Al_2O_3 composite coating is given. There is a single broad peak seen for as-plated Ni–B/Al_2O_3 composite coating. Apart from single broad peak, there are low intensity peaks present in the diffraction pattern. Low intensity peaks correspond to alumina. It can be concluded that the incorporation of alumina particles in Ni–B matrix has no important effect on the structure of the composite coatings. Many low intensity reflections are present in the case of XRD pattern obtained for composite coating (figure 5b). The deposits reveal a single broad peak corresponding to Ni (111) peak of a face-centred cubic (fcc) phase of nickel. This indicates the amorphous nature of the deposits. The XRD spectra of Ni–B/Al_2O_3 coating are similar to the others. XRD result for the Ni–B/Al_2O_3 coatings shows the phase points Ni (111) at $2\theta \approx 43.64°$, Ni (110) at $2\theta \approx 44.48°$, Ni (200) at $2\theta \approx 50.82°$, Ni (220) at $2\theta \approx 74.68°$ and Ni (311) at $2\theta \approx 90.7°$ (figure 5b).

The surface morphology of Ni–B and Ni–B/TiO_2 coatings as given in figure 6 exhibits coarse nodular compact structure (figure 6b). It can be seen that the surfaces of the substrate are fully covered with the electroless coatings, and the composite coating is composed of compact fine nodules of uniform size. Also the SEM images show that the coatings are uniform and non-porous in appearance. The inclusion of TiO_2 nanoparticles in Ni–B alloy matrix is achieved successfully from an electroless plating bath. The coating shows typical spherical nodular structures. Electroless Ni–B/TiO_2 coating has a 'clean' surface, and no clusters can be seen (figure 6b). For TiO_2 nanoparticles separated from composite coatings, the particles are much finer in the level of several nanometres.

The XRD patterns of Ni–B and Ni–B/TiO_2 coatings are compared (figure 6). The XRD spectrum in figure 6b confirms that amorphous anatase TiO_2 nanoparticles are dispersed in the composite coating. An interesting observation is that the phase structure of Ni–B/TiO_2 composite coatings is different from the coatings as shown by the XRD analysis (figure 6). A very weak TiO_2 peak is detected in the Ni–B/TiO_2 composite coating while no TiO_2 peaks can be seen from the new composite coatings, again probably due to the low quantity and highly dispersive distribution of the nano-sized TiO_2 particles. Unlike that of other coatings, the nodules are found to be less than 2.5 times (figure 6b). XRD result for the Ni–B/TiO_2 coatings is seen the phase points Ni

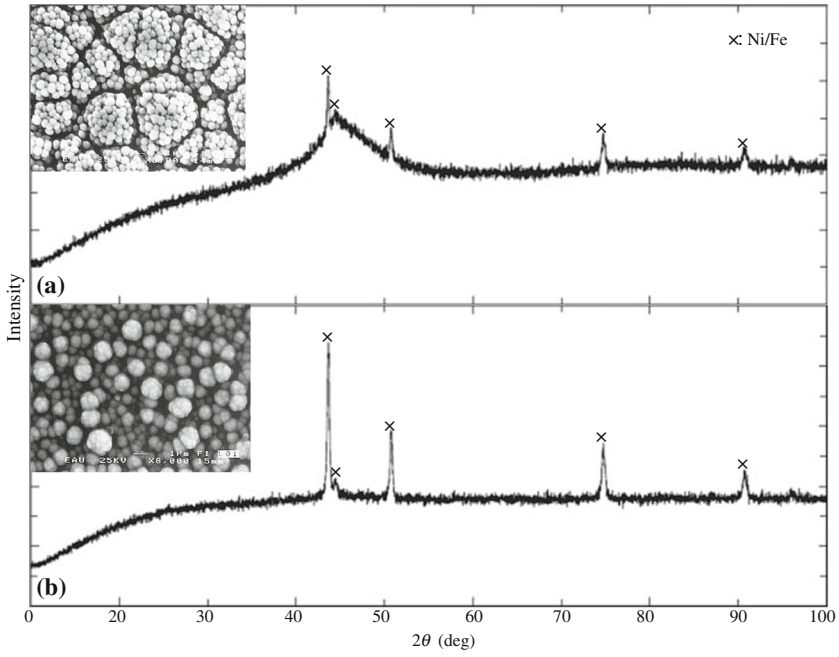

Figure 6. SEM images and XRD spectra of electroless (**a**) Ni–B and (**b**) Ni–B/TiO_2 composite coatings.

(111) at $2\theta \approx 43.66°$, Ni (110) at $2\theta \approx 44.46°$, Ni (200) at $2\theta \approx 50.78°$, Ni (220) at $2\theta \approx 74.72°$ and Ni (311) at $2\theta \approx 90.7°$ (figure 6b).

The SEM image of the Ni–B/CuO coating is seen similar to corn grains as shown in figure 7b. It has a nodule structure that consists of small grains, and exhibits a smooth surface and a specific geometry. The nodule size of CuO-reinforced electroless Ni–B coating is the largest. The nodule size of TiO_2-reinforced electroless Ni–B coating is the smallest. One reasons for this may be from diversity of coating thickness, because as coating thickness increases, nodule size also increases.[13] With the increase in Ni–B nanolayer thickness, Ni–B nodules appear in-between the mesh-like, seemingly porous Ni–B nanolayer structures and the nodule size grows with the nanolayer thickness. When the newly reduced Ni and B species continuously deposit on the Ni–B nanolayer itself at proximate locations, Ni–B nodules form but in a more mesh-like morphology than that formed under over-activated conditions. However, the nanolayer growth mode requires the diffusion of Ni and B species to the growing layer edge.[14] Since some Ni and B will not have enough time to diffuse long distance and attach to the growing layer edge before the arrival of the more reduced species, these diffusing species will adsorb on the top of the previously deposited Ni–B layer.[15] This leads to localized nodule growth or island-like nodule growth. Furthermore, some of the larger nodules or thicker locations that may appear on the surface are often associated with defects in the substrate that have attracted early nucleation and faster growth.[16–19] The thin locations are likely contributed by the porous locations of the nanolayer.[14] We may suggest that the size of the surface nodules was not constant during deposition. Consequently, the deposition process is a succession of germination phases (during which small nodules are formed), and growth phases (during which the formed entities become larger). A short induction period before any nickel is deposited, followed by a period during which some is deposited, but not yet in the form of observable nodules. The germination, and then growth of nodules, takes a balloon-like shape. This result is confirmed in Vitry *et al*.[20]

Zhong *et al*[21] in their patent explain that controlled introduction of copper ions activates natural nucleation sites and retards the nodule growth, such that the Ni–P coating is formed in a fine nodule size, exhibiting a significantly uniform microstructure and component distribution. Nodular deposition in a coating depends on the nucleation rate and the growth of the deposit. Nucleation rate depends on the bath pH, temperature, composition and impurities in it. The growth of the deposit is a function of the concentration of plating ingredients. Introduction of copper in the deposit seems to suppress the growth of the nodules by inhibiting further growth. This could be the main reason for obtaining bright and very smooth deposits of quaternary Ni–W–Cu–P alloys.[22]

XRD result for the Ni–B/CuO coatings is seen the phase points Ni_xB_y at $2\theta \approx 37°$, Ni (111) at $2\theta \approx 43.38°$, Ni (110) at $2\theta \approx 44.46°$, Ni (200) at $2\theta \approx 50.5°$, Ni (220) at $2\theta \approx 74.16°$ and Ni (311) at $2\theta \approx 90.06°$. However, it was found Ni_xB_y phase at $2\theta = 37°$ are not like other coatings and the highest the density of Ni (111) phase at $2\theta = 43.38°$ (figure 7b).

3.2 *Microhardness of coatings*

The microhardness of the substrate and coatings was measured using a Struers Duramin Vickers diamond indenter at

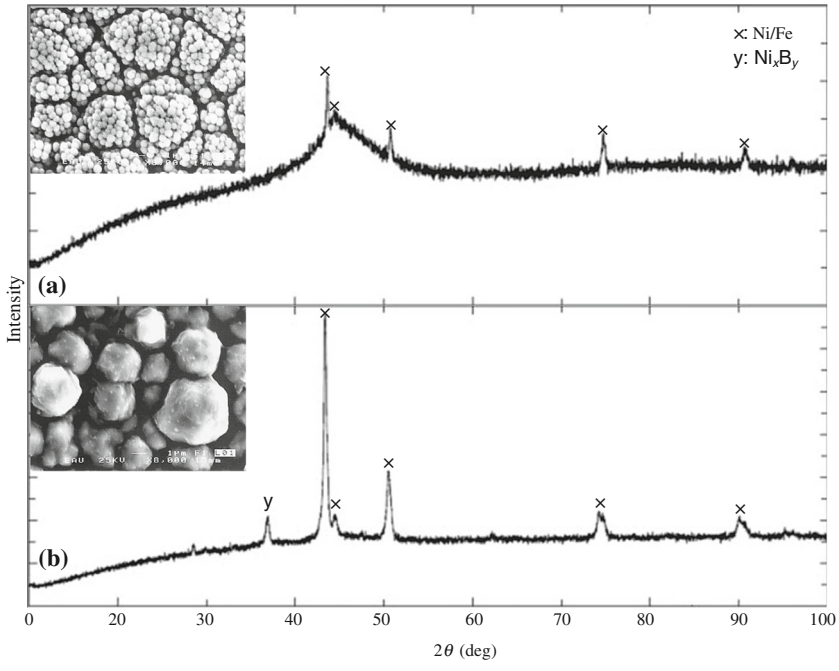

Figure 7. SEM images and XRD spectra of electroless (**a**) Ni–B and (**b**) Ni–B/CuO composite coatings.

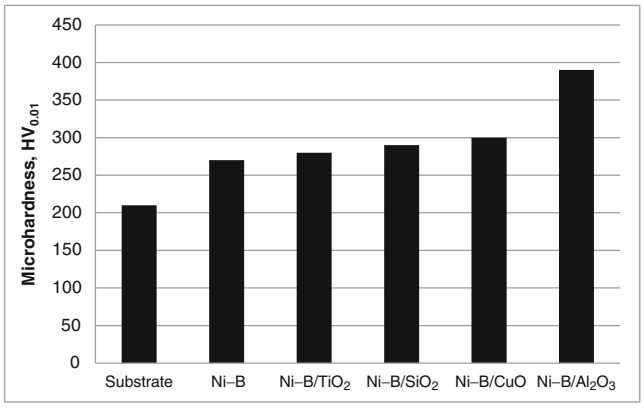

Figure 8. Microhardness of substrate and coatings.

a load of 10 g for a loading time of 10 s. An average of six measurements was reported as the microhardness value. This coating process resulted in a significantly improved microhardness. Microhardness results are graphitized in figure 8. According to this, the microhardness values of the substrate, electroless Ni–B, Ni–B/TiO_2, Ni–B/SiO_2, Ni–B/CuO and Ni–B/Al_2O_3 composite coatings can be sorted in ascending order (210, 270, 280, 290, 300 and 390 $HV_{0.01}$, respectively). It is seen that nanoparticles act as crystals which enhance hardness. The reinforcement of nanoparticles dispersed in the matrix by many possible hardening mechanisms can be explained. One of them may be the dispersion strengthening of the matrix.[23] It may be that the nanoparticles hinder the grain boundary-mediated processes.[24] In this case, it is believed that the matrix carries the compressive force while the dispersed particles obstruct the dislocation motion. It also should be noted that based on results from Gül *et al*.[25] Also, according to Ranade *et al*,[26] the formation of coherent matrix–nanoparticle interfaces produce stress fields activating the motion of nearby dislocations within the matrix, and improves mechanical property. Weiwei *et al*[6] also have reported that introducing nanoparticles by adding the solution can effectively avoid particle agglomeration, therefore significantly improving the particle dispersion strengthening effect explained by Orowan mechanism. The microhardness of Ni–B/Al_2O_3 composite coating is the highest according to that of others. However, the nanocomposite coating with the lowest hardness is Ni–B/TiO_2. This difference can be attributed to the greater compressive strength and modulus of elasticity of Al_2O_3 particles compared with TiO_2. It is confirmed by Farrokhzad and Khan.[23]

4. Conclusions

From the present paper, it can be seen that electroless nickel–boron composite coatings have emerged as suitable coatings that can serve as viable replacements to the conventional electroplating in suitable situations. The uniform deposition and the ability to coat any materials serve as an added advantage to their application in various areas. By observing the expansion possibilities of electroless nickel–boron composite coatings, more advanced tribological application of the coatings may be expected. Microstructural characterization of the coatings is important as it helps to better understand its macroscopic behaviour by observing the changes occurring at the microscopic level of the coating, because, depending on the characteristics of the microstructure and crystal structure varies the hardness, tribological and corrosion properties of coatings. In this paper, we made a thorough study about the growth morphology and crystallinity of electroless Ni–B/SiO_2, Al_2O_3, TiO_2 composite coatings. The SEM images of electroless Ni–B and Ni–B/nanocomposite coatings show different microstructures. The grains of coatings are found in the form of nodule. These nodules are observed in the form of blackberry at Ni–B/TiO_2, cauliflower, grapes at Ni–B/Al_2O_3 and corn grains at Ni–B/CuO in the microstructure of coatings. It is found that Ni–B/TiO_2 has the smallest nodule with 1.6 μm and Ni–B/CuO the largest nodule with 6 μm when compared in terms of nodule size. Electroless Ni–B and Ni–B/nanocomposite coatings show Ni/Fe peaks consisting of the substrate material. However, the XRD spectrum of electroless Ni–B/CuO coating signs Ni_xB_y phase at $2\theta = 37°$ unlike other coatings. It is found to be the most intensive when compared to other coatings Ni (110) peak at $2\theta = 44.48°$ in the Ni–B/Al_2O_3 coating and at Ni (111) peak at $2\theta = 43.38°$ in the Ni–B/CuO coating. The XRD spectra of coatings Ni–B/TiO_2 and Ni–B/Al_2O_3 do not change significantly. Phase structure of the coatings remains almost the same. Electroless Ni–B and Ni–B/nanocomposite coatings shield Ni/Fe peaks which formed the substrate material.

The incorporation of nanoparticles in nickel–boron matrix increases the hardness of coatings. Electroless Ni–B/nanocomposite coatings exhibit higher hardness as compared with electroless Ni–B coating, which can be attributed to especially the traditional dispersion-strengthening mechanism.

Acknowledgements

The study was supported by Atatürk University Research Funding BAP by a Grant no. 2012/118. We would like to thank Atatürk University for funding the project.

References

1. Bulbul F 2011 *Met. Mater. Int.* **17** 67
2. Dong D, Chen X H, Xiao W T, Yang G B and Zhang P Y 2009 *Appl. Surf. Sci.* **255** 7051
3. Sadreddini S and Afshar A 2014 *Appl. Surf. Sci.* **303** 125
4. Hu X, Xu S, Yang Y, Chen Z and Chan Y C 2014 *Mater. Sci. Eng.* **A600** 67
5. Novakovic J, Vassiliou P, Samara K l and Argyropoulos Th 2006 *Surf. Coat. Technol.* **201** 895
6. Weiwei C, Gao W and He Y 2010 *Surf. Coat. Technol.* **204** 2493
7. De Hazan Y, Werner D, Z'graggen M, Groteklaes M and Graule T 2008 *J. Colloid Interface Sci.* **328** 103

8. Balaraju J N, Kalavati and Rajam K S 2006 *Surf. Coat. Technol.* **200** 3933
9. Li C, Wang Y and Pan Z 2013 *Mater. Des.* **47** 443
10. Fiori F, Girardin E, Albertini G, Konopka K and Rustichelli F 2008 *Mater. Sci. Eng.* **B152** 136
11. Bülbül F, Altun H, Küçük Ö and Ezirmik V 2012 *Met. Mater. Int.* **18** 631
12. Rabizadeh T and Allahkaram S R 2011 *Mater. Des.* **32** 133
13. Schwartz M M 2002 *Encyclopedia of materials, parts and finishes* (Florida: CRC Press) 2nd ed., p 139
14. Zhu X 2008 *Processability of nickel–boron nanolayer coated boron carbide* Ph.D. Thesis (Virginia: Virginia Polytechnic Institute and State University)
15. Mathur S and Singh M 2009 *Nanostructured materials and nanotechnology* (New Jersey: John Wiley & Sons) vol. 2, p 117
16. Spalvins T and Brainard W A 1974 *J. Vac. Sci. Technol.* **11** 1186
17. Czigany Zs and Radnoczi G 1999 *Thin Solid Films* **343** 5
18. Bochkarev A A, Poliakova V I and Pukhovoy M V 1999 *Thin Solid Films* **343** 9
19. Guenther K H 1984 *Appl. Opt.* **23** 3806
20. Vitry V, Sens A, Kanta A F and Delaunois F 2012 *Appl. Surf. Sci.* **263** 640
21. Zhong L L, Liu C C and John J D 2002 *Electroless nickel–phosphorus coatings with high thermal stability* Patent US6410104 B1 (Seagate Technology Llc)
22. Balaraju J N and Rajam K S 2005 *Surf. Coat. Technol.* **195** 159
23. Farrokhzad M A and Khan T I 2014 *Adv. Compos. Mater.* **24** 141
24. Bakhit B and Akbari A 2013 *J. Alloys Compd.* **560** 92
25. Gül H, Kilic F, Aslan S, Alp A and Akbulut H 2009 *Wear* **267** 976
26. Ranade A N, Krishna L R, Li Z, Wang J, Korach C S and Chung Y W 2012 *Surf. Coat. Technol.* **213** 26